Nanoscale

RSC Publishing

PAPER

View Article Online
View Journal | View Issue

Cite this: *Nanoscale*, 2013, **5**, 7312

Hierarchical composites of polyaniline–graphene nanoribbons–carbon nanotubes as electrode materials in all-solid-state supercapacitors

Mingkai Liu,[a] Yue-E Miao,[a] Chao Zhang,[a] Weng Weei Tjiu,[b] Zhibin Yang,[a] Huisheng Peng[a] and Tianxi Liu*[a]

A three dimensional (3D) polyaniline (PANI)–graphene nanoribbon (GNR)–carbon nanotube (CNT) composite, PANI–GNR–CNT, has been prepared *via in situ* polymerization of an aniline monomer on the surface of a GNR–CNT hybrid. Here, the 3D GNR–CNT hybrid has been conveniently prepared by partially unzipping the pristine multi-walled CNTs, while the residual CNTs act as "bridges" connecting different GNRs. The morphology and structure of the resulting hybrid materials have been characterized using transmission electron microscopy (TEM), scanning electron microscopy (SEM), Raman spectroscopy and X-ray diffraction (XRD). Electrochemical tests reveal that the hierarchical PANI–GNR–CNT composite based on the two-electrode cell possesses much higher specific capacitance (890 F g^{-1}) than the GNR–CNT hybrid (195 F g^{-1}) and neat PANI (283 F g^{-1}) at a discharge current density of 0.5 A g^{-1}. At the same time, the PANI–GNR–CNT composite displays good cycling stability with a retention ratio of 89% after 1000 cycles, suggesting that this novel PANI–GNR–CNT composite is a promising candidate for energy storage applications.

Received 23rd March 2013
Accepted 20th May 2013

DOI: 10.1039/c3nr01442h

www.rsc.org/nanoscale

1 Introduction

As one of the most important energy storage devices, electrochemical capacitors, also called supercapacitors, have attracted considerable attention due to their distinctive features such as high power density, long cycle life, fast charge–discharge capabilities as well as low maintenance cost.[1–5] Recently, in order to improve the electrochemical performance of the prepared devices, many attempts have been devoted to exploring novel hierarchical materials, which are crucial and indispensable for the electrochemical devices.[6–10] Among all the electrode materials, conducting polymers have been considered as one of the most promising electrode materials for supercapacitors owing to their low cost and simple synthesis, as well as their ability of storing charges both in the hybrid supercapacitor and pseudocapacitor.[11,12] Polyaniline (PANI) is the most widely used electrode material for supercapacitors due to its distinctive features such as high conductivity and excellent capacity for energy storage resulting from its multiple redox states.[13] However, due to its drawbacks of swelling and shrinkage during the doping–dedoping processes, PANI is susceptible to a rapid degradation in electrochemical performance upon repetitive cycles of charge–discharge,[14,15] resulting in a poor cycling stability.

In order to overcome these limitations, much attention has been devoted to preparing hybrid electrodes by combining PANI with other nanomaterials. For example, coupling carbon-based nanomaterials with PANI, such as graphene–PANI,[16,17] porous carbon–PANI[18] and carbon nanotube (CNT)–PANI composites,[19] has been confirmed to be an effective approach to improve the cycle life of PANI and further alleviate the limitation of its real applications. It needs to be emphasized that, among these carbon-based nanomaterials, carbonic hybrid materials consisting of graphene and CNTs have been shown to be one kind of ideal electrode material for supercapacitors, which effectively eliminates the contacting resistance inside the hybrid and achieves the synergistic effects of graphene and CNTs, resulting in a superior electrochemical performance compared with a single component of graphene or CNTs.[20,21]

Although the CNTs bonded on the surface of graphene have enlarged the contacting area and facilitated the electron transfer inside the composites, the hybrid materials prepared by a simple mixing of the graphene and CNTs cannot develop strong interactions between the two materials, and a homogeneously dispersed graphene–CNT hybrid cannot be achieved.[22] These factors hinder the formation of conductive pathways and result in a deterioration of the electrical conductivity of the graphene–CNT hybrid. Moreover, due to the drawbacks of high cost and

[a]*State Key Laboratory of Molecular Engineering of Polymers, Department of Macromolecular Science, Laboratory of Advanced Materials, Fudan University, Shanghai, 200433, P.R. China. E-mail: txliu@fudan.edu.cn; Fax: +86-21-65640293; Tel: +86-21-55664197*

[b]*Institute of Materials Research and Engineering, A*STAR (Agency for Science, Technology and Research), 3 Research Link, Singapore, 117602, Singapore*

complicated preparation processes, three-dimensional (3D) seamless graphene–CNT hybrids obtained by chemical vapor deposition cannot be made *via* mass production and meet the real needs of industrial production. These limitations further hinder the rapid development and full utilization of carbon-based hybrid materials.

In this work, we have prepared a carbon-based material, namely a graphene nanoribbon (GNR)–CNT hybrid by partially unzipping the multi-walled CNTs. Also, pure GNRs have been prepared by totally unzipping the pristine CNTs. For the GNR–CNT hybrid, with the CNTs bonded on different GNRs, the aggregation tendency of the GNRs has been effectively impeded by forming a 3D conductive network inside the hybrid, resulting in a highly enhanced electrical conductivity. With PANI uniformly polymerized on the surface of the GNR–CNT hybrid, a novel hierarchical PANI–GNR–CNT composite has been successfully prepared. Due to synergistic effects, the specific capacitance of the GNR–CNT hybrid has been dramatically increased. Moreover, the cycle life of PANI has been greatly enhanced by incorporating GNR–CNT hybrid into the composite.

2 Experimental section

2.1 Sample preparation

GNRs were synthesized by unzipping the CNTs (diameter of 40–60 nm, Chengdu Organic Chemicals Co. Ltd.) and subsequently reduced using hydriodic acid. The GNR–CNT hybrid was prepared by partially unzipping the pristine CNTs (with an adequate amount of oxidizing reagents of potassium permanganate ($KMnO_4$)) and subsequently reduced using the hydriodic acid. The unzipping method was employed here according to the modified Tour method.[23,24] Typically, 500 mg of CNTs and 100 mL of concentrated sulfuric acid (98%) were mixed by continuous stirring in a 500 mL flask. After 1 h, 13 mL of phosphoric acid (H_3PO_4) (30%) was added into the mixture. Then, 1.5 g (or 3 g) $KMnO_4$ was added into the reaction system in batches of 0.5 g per 30 min. After the reaction was finished, the mixture was naturally cooled to room temperature and subsequently poured into 1 L of ice-water containing 15 mL H_2O_2 (30 wt%). The mixture was allowed to coagulate for 24 h and the precipitate was sonicated for 20 min with a power of 100 W. Afterwards, the obtained samples were dialyzed for one week. Then, the oxidized GNRs (or GNR–CNT hybrid) thus obtained were reduced using hydriodic acid at 100 °C for 10 h to obtain the GNRs or GNR–CNT hybrid. Hierarchical composites of PANI–GNR and PANI–GNR–CNT were synthesized by *in situ* polymerization of an aniline monomer on the surface of the GNRs (or GNR–CNT hybrid). Typically, 50 mg of GNRs (or the GNR–CNT hybrid) were dispersed in 50 mL of deionized (DI) water. After being sonicated for 2 h, 50 mL of 0.2 M aniline monomer dissolved in 1 M HCl solution was added and the mixture was continuously stirred for 0.5 h in ice bath. Then 0.1 M ammonium persulfate (APS) dissolved in 50 mL of 1 M HCl solution was slowly added into the mixture dropwise. The mixture was stirred overnight and the resulting precipitates were washed with DI water several times. The mass fraction of PANI calculated from the weight of the GNRs (or GNR–CNT hybrid) before and after polymerization was 95%. Composites of PANI–GNR and PANI–GNR–CNT with different weight percents of PANI were also prepared by varying the amount of aniline monomer used in the polymerization process. In addition, the composite of PANI–CNT was fabricated by *in situ* polymerization of an aniline monomer on the surface of acid-treated CNTs, which were surface-modified by a 3 : 1 mixture of concentrated H_2SO_4 : HNO_3, as reported elsewhere.[25,26] Furthermore, pure PANI was synthesized through the above chemical process without the presence of a GNR or GNR–CNT suspension for comparison.

2.2 Characterization

Transmission electron microscopy (TEM) observations were performed on a Jeol JEM 2100 TEM instrument with an accelerating voltage of 200 kV. A field emission scanning electron microscope (FESEM, JEOL JSM-6700F) was used to observe the morphology of the surface of the samples. X-ray diffraction (XRD) measurements were recorded on an XRD system (D8-Advance, Germany) equipped with Cu-Kα radiation. Raman spectra were collected using an Avalon Instruments Raman Station with a 632.8 nm He–Ne laser. The electrical conductivity of the prepared samples was tested using a 4-Point Probes Resistivity Measurement System (RTS-8).

2.3 Fabrication of supercapacitor electrodes

Here the all-solid-state supercapacitor cells were fabricated as a two-electrode system. The same amounts of the as-prepared electrode materials were respectively coated on the surface of two pieces of fluorine-doped tin oxide (FTO) and used as electrodes to fabricate symmetric supercapacitors. Poly(vinyl alcohol) (PVA)–H_3PO_4 gel prepared by dissolving PVA powder (1 g) in DI water (10 mL) and 30% H_3PO_4 (2 mL) was directly used as the electrolyte which was sandwiched between the two electrodes.

2.4 Electrochemical measurements

The electrochemical properties of supercapacitor electrodes were investigated in a two-electrode system by cyclic voltammetry (CV), galvanostatic charge–discharge measurements, and electrochemical impedance spectroscopy (EIS) using a CHI 660D electrochemical workstation (Shanghai Chenhua, China). CV response of the electrodes was measured at different scan rates varying from 5 to 100 mV s^{-1} over a potential range from −0.2 to 1.0 V. The potential range for the charge–discharge tests was between 0 and 0.8 V. Impedance spectroscopy measurements were conducted out at a bias potential of 0.5 V with a potential amplitude of 5 mV and frequency ranging from 100 kHz to 0.01 Hz.

The specific capacitance (C_{sp}) of the all-solid-state supercapacitor cell in a two-electrode system was calculated using the following eqn (1):

$$C_{sp} = 4I\Delta t/m\Delta E \quad (1)$$

where C_{sp} is the specific capacitance, I is the discharge current (A), m is the total mass of the active electrode materials on two sides (g), Δt is the discharge time (s), and ΔE denotes the voltage difference (V).

3 Results and discussion

Fig. 1 shows the TEM images of the pristine CNTs, GNR–CNT hybrid and pure GNR sheets at low and high magnifications. Compared with pristine CNTs (Fig. 1a), the partially unzipped GNR–CNT hybrid (Fig. 1b) apparently consists of two components: opened GNRs and residual CNTs with smaller diameters (as indicated by the arrows). With further careful unzipping treatment, the pristine CNTs can be totally opened, resulting in the formation of pure GNRs, as shown in Fig. 1c. It is evident that the opened GNRs have a much broader width than the residual CNTs, and a comparable length to that of the CNTs even after being treated by sonication. Fig. 1e shows the TEM image of the GNR–CNT hybrid at high magnification in which residual CNTs co-existing with the unzipped GNRs can be obviously observed. Moreover, the obtained GNRs can be closely integrated with the residual CNTs due to the presence of interfacial interactions (*i.e.*, the π–π interaction).[27] It can be also observed that the obtained GNRs are connected together, which efficiently increases the contact area between different GNRs (as seen in Fig. 1c), facilitating the formation of a conductive pathway. Fig. 1f provides more detail on the structure and morphology of the GNRs. It can be seen that different GNRs are connected by bonding their surfaces to each other, which builds up an ideal conductive pathway inside the GNR samples. The electrically conductive properties of the prepared materials have been investigated by a four-point probe method. Most interestingly, the GNR–CNT hybrid exhibits a much higher electrically conductivity (180 S cm^{-1}) than the obtained GNRs (85 S cm^{-1}) and pristine CNTs (65 S cm^{-1}). This improved conductive property can be ascribed to the synergistic enhancement effect of the GNR sheets and residual CNTs, as a 3D carbonic hybrid with a unique morphology has been

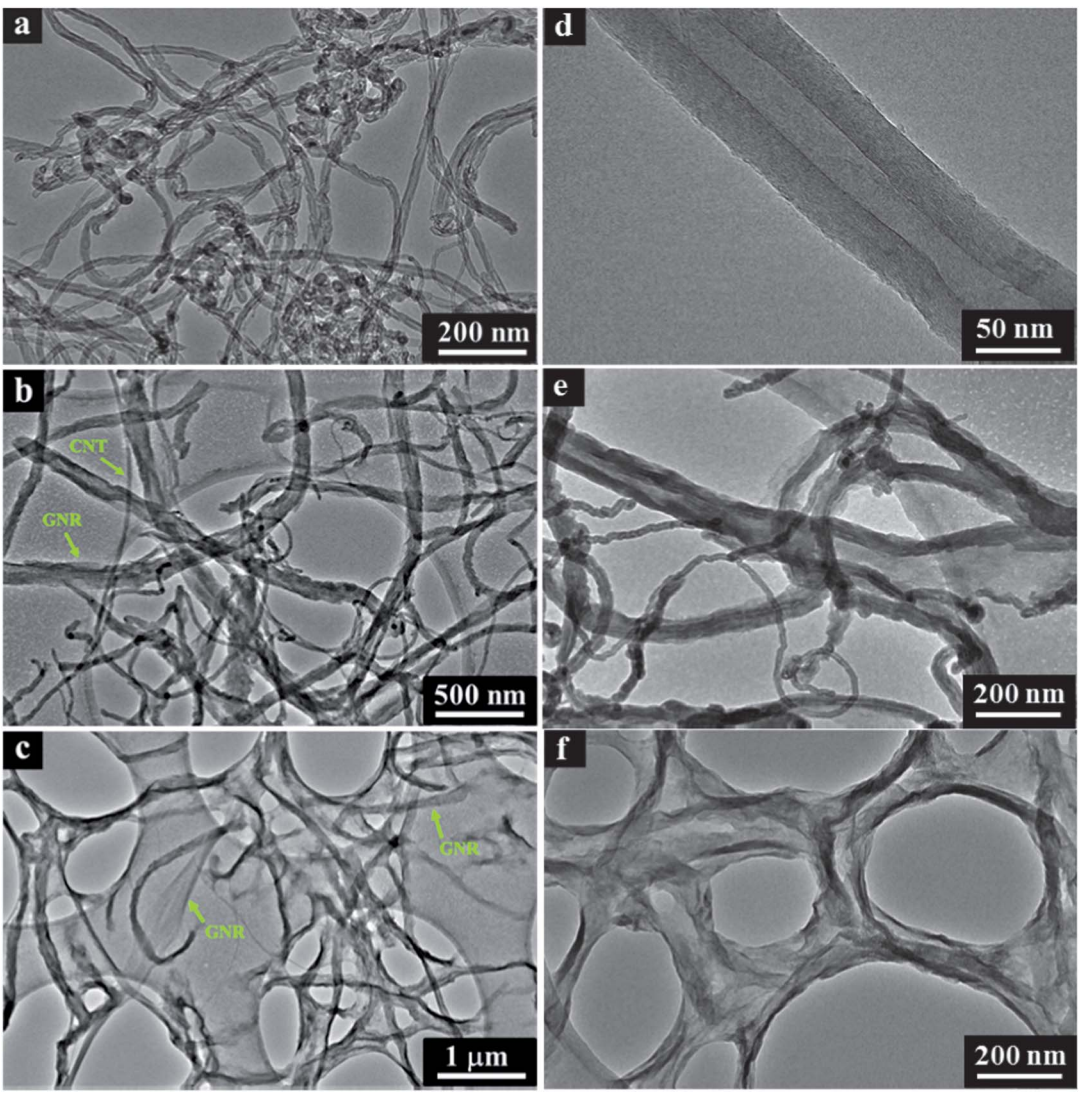

Fig. 1 TEM images of (a and d) pristine CNTs, (b and e) GNR–CNT hybrid and (c and f) pure GNR sheets at low and high magnifications.

constructed by bonding the residual CNTs on the opened GNR sheets, which can greatly decrease the contacting resistance between the GNR sheets by establishing much more conductive pathways inside the GNR–CNT hybrid.[28] Furthermore, with the existence and assistance of the residual CNTs, the GNR–CNT hybrid can achieve a better porous or open structure than the pure GNRs as the CNTs inside the GNR–CNT hybrid can act as "skeletons" between different GNRs, thus preventing close stacking between different GNR sheets (as seen in Fig. 1e and f). The improved conductive properties and formation of porous structure in the GNR–CNT hybrid will be expected to further promote the electrochemical performance of the supercapacitor.

The morphology of the as-prepared materials was further observed using SEM (as seen in Fig. 2). Fig. 2a and b show the morphologies of the GNR–CNT hybrid and pure GNRs. Compared with the GNRs, it can be clearly observed that there are some residual CNTs in the GNR–CNT hybrid, acting as the bridges between different GNRs to form a conductive network. With PANI uniformly grown on the surfaces of GNRs and GNR–CNT hybrid, PANI–GNR and PANI–GNR–CNT composites were obtained (Fig. 2c and d). The neat PANI shows a rod-like particle morphology (Fig. 2e), which seems to be loosely packed and forms short rod-like structures. Because of the rod-like morphology and high coverage of PANI as well as the low dimensional features of the GNRs, the structure of the GNRs in the PANI–GNR composites cannot be observed clearly. However, for the PANI–GNR–CNT composite, the existence of the CNTs can be clearly observed although the structure of the GNRs is still unclear. Since the GNRs unzipped from the pristine CNTs have more carboxylic groups than the residual CNTs, it can be supposed that the positively charged aniline monomers are prone to be adsorbed on the surfaces of the negatively charged GNRs.[11] The aniline molecules are prompted to polymerize from the adsorbed sites on the GNR surfaces when APS is added into the suspension, which results in a close contact between the GNRs and PANI, thus effectively decreasing the resistance to charge transfer between the GNRs and PANI. Furthermore, the residual CNTs act as conductive bridges interconnecting among the PANI–GNR composite particles, beneficially improving the electrical conductivity of the composite.

To further study the interaction between these carbonic materials and PANI, Raman spectroscopy analysis is employed. The Raman spectra of the pristine CNTs, GNRs, GNR–CNT hybrid, neat PANI, PANI–GNR and PANI–GNR–CNT composites are presented in Fig. 3. In the low wavenumber region from 100 to 1000 cm^{-1}, the carbonic materials show smooth curves without any peaks, which is in good agreement with the literature.[29,30] Compared with neat PANI, the PANI–GNR and PANI–GNR–CNT composites show apparent peaks in the low wavenumber regions of different intensities and sharpness. The band at about 420 cm^{-1} can be ascribed to out-of-plane amine ring deformations,[25] and the band at about 575 cm^{-1} is an identification of the existence of ring deformation and phenazine- or phenoxazine-like segments, whereas the bands around 780 and 820 cm^{-1} correspond to amine and imine deformation (C–N–C bending).[31] In the high wavenumber regions, the Raman spectra of the pristine CNTs, GNRs, and GNR–CNT hybrid show the distinctive peaks of the D band and G band which respectively correspond to the breathing modes of the rings or the *K*-point phonons of A_{1g} symmetry and E_{2g} phonons.[32] However, the PANI–GNR and PANI–GNR–CNT composites show sharp peaks at about 1180 cm^{-1}, which represents the C–H bending in the

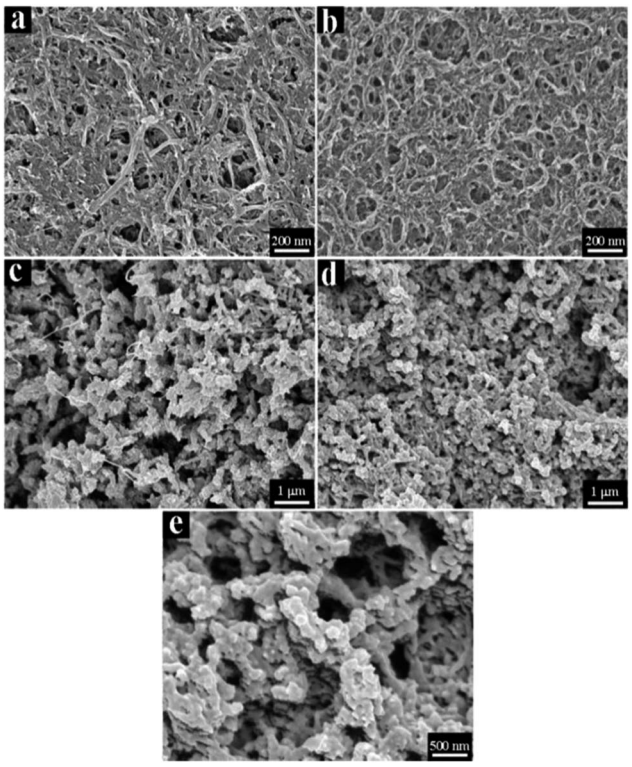

Fig. 2 SEM images of the (a) GNR–CNT hybrid, (b) GNRs, (c) PANI–GNR–CNT composite, (d) PANI–GNR composite, and (e) neat PANI.

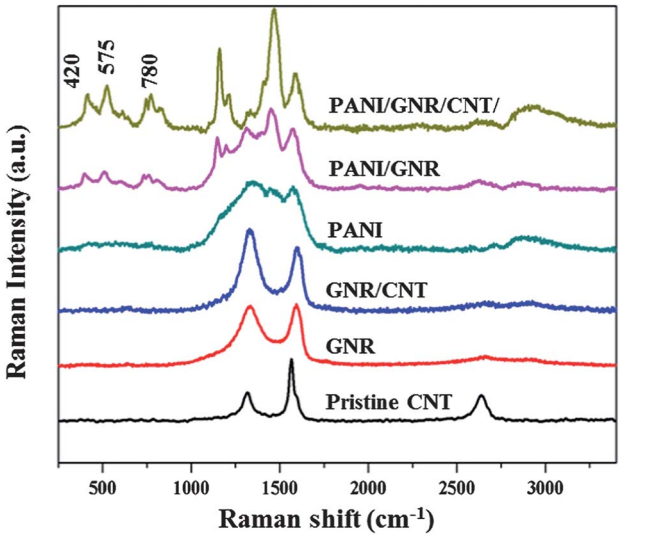

Fig. 3 Raman spectra of pristine CNTs, GNRs, GNR–CNT hybrid, neat PANI, PANI/GNR and PANI–GNR–CNT composites.

benzene- or quinine-type rings. The peak at 1350 cm^{-1} is a clear indication of C–N^+ stretching, and the one at 1485 cm^{-1} reveals the C=N stretching vibration in the emeraldine base of imines resulting from the n-doping effect of PANI. The Raman results further confirm that the hybrid material of PANI–GNR–CNT with strong π–π interactions has been successfully synthesized.[33,34]

The XRD patterns of the GNRs, GNR–CNT hybrid and their PANI composites are shown in Fig. 4. The GNRs exhibit a broad peak at about $2\theta = 25.8°$, corresponding to a *d*-spacing of 3.5 Å, which is consistent with the results for graphene.[24,27] However, the GNR–CNT hybrid shows a weak and broad peak at $2\theta = 24.5°$, which can be ascribed to the existence of the residual CNTs. For neat PANI, the crystalline peaks appearing at $2\theta = 15.2°$, 20.7°, 25.2°, correspond to the (011), (020) and (200) crystal planes in its emeraldine salt form, respectively.[35] Moreover, the X-ray data of the PANI–GNR and PANI–GNR–CNT composites show similar crystalline peaks to that of neat PANI, indicating that the PANI grown on the surfaces of the carbonic materials possesses good crystalline properties which are not affected by the incorporation of a small amount (5 wt%) of GNRs or GNR–CNT hybrids.[29,36]

Furthermore, in order to confirm the fact that the pristine CNTs were successfully partially or totally unzipped, XRD analyses of the oxide GNR–CNT hybrid and oxide GNRs were performed, as seen in Fig. 5. Compared with the pristine CNTs, the XRD pattern of the oxide GNRs shows a characteristic diffraction peak at $2\theta = 12.5°$, which is similar to the X-ray data for graphene, indicating that the pristine CNTs have been totally opened. However, the XRD pattern of the oxide GNR–CNT hybrid shows two obvious diffraction peaks at $2\theta = 12.5°$ and 25.8°, which indicates the co-existence of the oxide GNRs and the residual CNTs in the oxide GNR–CNT hybrid.

In order to evaluate the electrochemical performance of the supercapacitor cells based on the obtained materials, CV and galvanostatic charge–discharge measurements were performed in a two electrode system. Fig. 6a shows the CV curves of the

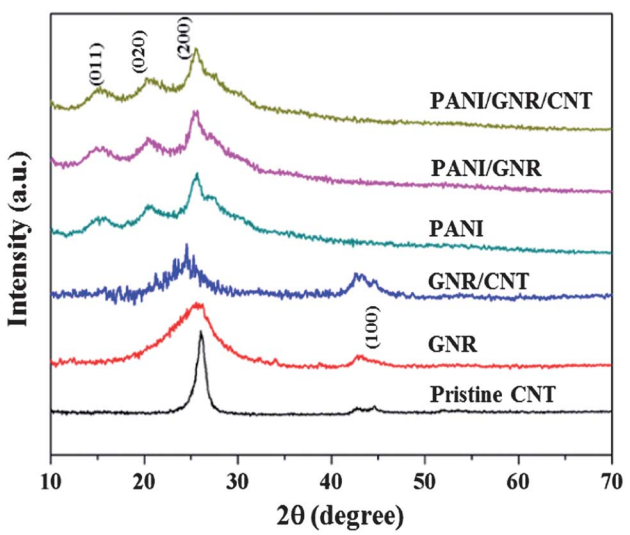

Fig. 4 XRD patterns of the CNT, as-prepared GNRs, GNR–CNT hybrid, neat PANI, PANI–GNR and PANI–GNR–CNT composite samples.

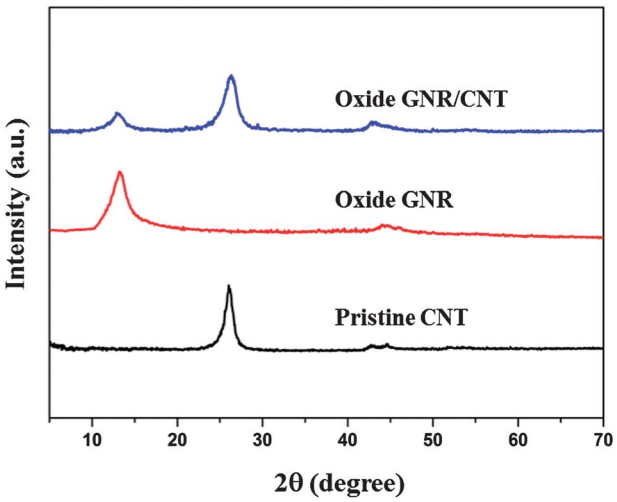

Fig. 5 XRD patterns of oxide GNR–CNT, oxide GNR and pristine CNT.

pristine CNTs, GNRs, GNR–CNT hybrid, neat PANI, PANI–GNR and PANI–GNR–CNT composites. It can be seen that the CV curves of the pristine CNTs, GNRs and GNR–CNT hybrid show approximately rectangular shapes which is characteristic for an electrical double layer capacitor (EDLC),[37,38] whereas the CV curves of the neat PANI, PANI–GNR and PANI–GNR–CNT composites clearly exhibit three pairs of redox peaks from −0.2 to 1.0 V, which are an indication of a typical pseudocapacitive characteristic of PANI.[39,40] It can also be seen that the area surrounded by the CV curve of the PANI–GNR–CNT composite is larger than those of the neat PANI, PANI–GNR composite and the GNR–CNT hybrid at the same scan rate, indicating a higher specific capacitance. PANI in the composites can provide a pseudocapacitive action and enhance the electrode–electrolyte interface area, which enables the electrochemical accessibility to the electrolyte through the loosely packed PANI fibrous structure.[14] With the GNRs as the support material for the polymerization of the aniline monomer, the transport of the electrolyte ions in the electrode is greatly facilitated during charge–discharge processes. As the CV curve of the PANI–GNR–CNT composite is different but larger than those of the neat PANI and GNR–CNT hybrid, it can be supposed that the PANI–GNR–CNT composite has realized the synergistic effects of the PANI and GNR–CNT hybrid. Furthermore, with the residual CNTs acting as electrically conductive bridges inside the PANI–GNR–CNT composite, the diffusion length of the electrolyte ions is greatly reduced, resulting in an enhanced CV curve compared to that of the PANI–GNR composite, which means a higher specific capacitance of the PANI–GNR–CNT composite.

Fig. 6b shows the galvanostatic charge–discharge curves of the samples at a current density of 0.5 A g^{-1}. The pristine CNT, GNR and GNR–CNT hybrid electrodes show triangular-shape charge–discharge curves, indicating that the capacitance is mainly from the EDLC. However, the galvanostatic charge–discharge plots of PANI, PANI–GNR and PANI–GNR–CNT composite electrodes exhibit a capacitive behavior with almost symmetric charge–discharge curves, where the deviation to linearity is typical of a pseudocapacitive contribution.[41] The

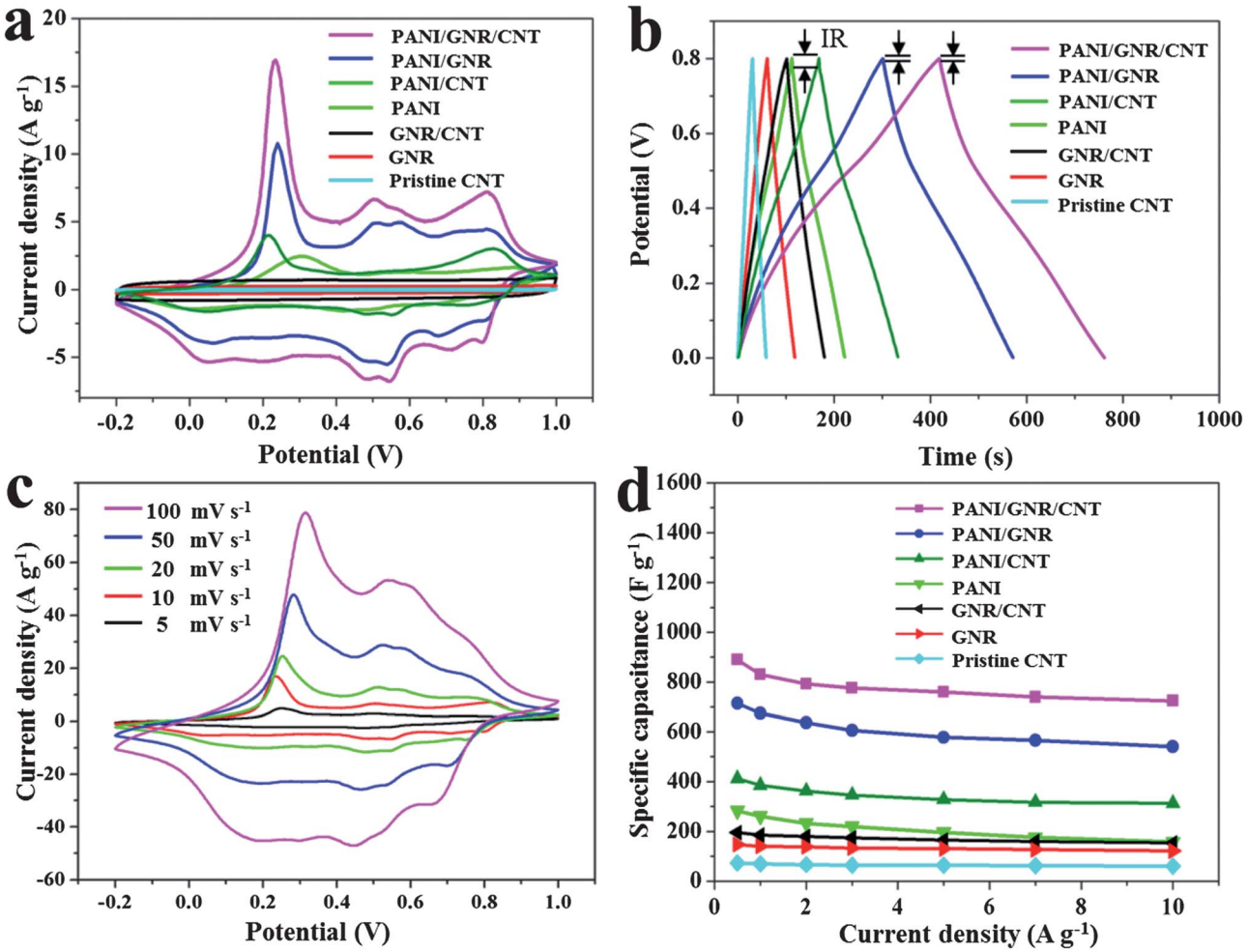

Fig. 6 (a) CV curves of the pristine CNTs, GNRs, GNR–CNT hybrid, neat PANI, PANI–CNT, PANI–GNR and PANI–GNR–CNT composites at 10 mV s^{-1} in 1 M H_2SO_4 solution; (b) galvanostatic charge–discharge curves of the GNRs, GNR–CNT hybrid, neat PANI, PANI–CNT, PANI–GNR and PANI–GNR–CNT composites at 0.5 A g^{-1}; (c) CV curves of the PANI–GNR–CNT composite at different scan rates of 5, 10, 20, 50 and 100 mV s^{-1}; (d) specific capacitance of the GNRs, GNR–CNT hybrid, neat PANI, PANI–CNT, PANI–GNR and PANI–GNR–CNT composites as a function of current density.

"IR drop" of the PANI–GNR and PANI–GNR–CNT composites is lower than that of PANI, reflecting the fact that the internal resistance of the PANI–GNR and PANI–GNR–CNT composites is greatly decreased by incorporating the GNRs and GNR–CNT hybrid. Due to this lower internal resistance, less energy in the devices will be wasted to produce unwanted heat during charge–discharge processes.[42] The charge–discharge duration of the PANI–GNR–CNT composite is much larger than those of the other electrode materials prepared here, implying the highest specific capacitance for the PANI–GNR–CNT composite and also confirming that the synergistic effect has been realized in the PANI–GNR–CNT composite. Additionally, the specific capacitance (890 F g^{-1}) of the PANI–GNR–CNT composite electrode is higher than that of the PANI–GNR electrode (714 F g^{-1}), which can be attributed to the presence of the residual CNTs inside the PANI–GNR–CNT composite. The residual CNTs not only aid the charge transfer inside the ternary composite but also decrease the internal resistance of the electrode. These results are in accordance with those deduced from the CV tests. Fig. 6c shows the CV curves of the PANI–GNR–CNT composite electrode at different scan rates. It is notable that the composite exhibits excellent electrochemical behavior in a wide range of scan rates from 5 to 100 mV s^{-1}, and an obvious increase of current with scan rate indicates a good rate capability for the PANI–GNR–CNT composite electrode.

Fig. 6d shows the specific capacitance of the prepared electrode materials as a function of discharge current density. The specific capacitance of the PANI–GNR–CNT and PANI–GNR composites is much higher than those of the pristine CNTs, neat PANI, GNRs and GNR–CNT hybrid under the same current density. It can be observed that the maximum specific capacitance (890 F g^{-1}) of the PANI–GNR–CNT composite measured at a current density of 0.5 A g^{-1} is much higher than those of the neat PANI (283 F g^{-1}), pristine CNTs (73 F g^{-1}), GNRs (147 F g^{-1}), GNR–CNT hybrid (195 F g^{-1}), PANI–CNT (412 F g^{-1}) and PANI–GNR composite (714 F g^{-1}). This greatly enhanced specific capacitance of the PANI–GNR–CNT composite could be due to the presence of the GNR–CNT hybrid which can provide a high specific surface area and good electrical conductivity and can be associated with the good redox activity of the PANI.

EIS analysis is a powerful technique to evaluate the properties of electrode materials, such as conductivity, structure and charge transport in the electrode materials/electrolyte interface.[4] Fig. 7a shows the Nyquist plots of the neat PANI, PANI–GNR and PANI–GNR–CNT composites and the GNR–CNT hybrid. Compared with neat PANI, the Nyquist plots of the PANI–GNR and PANI–GNR–CNT composites and the GNR–CNT hybrid show more vertical lines in the low-frequency region and more inconspicuous arcs in the high-frequency region. These vertical shapes at lower frequencies indicate better capacitive behaviors and lower ion diffusion resistance because the more vertical the curve, the more closely the supercapacitor behaves as an ideal capacitor.[43] The inconspicuous arcs in the high-frequency region confirm the low electronic resistance of the PANI–GNR and PANI–GNR–CNT composites and GNR–CNT hybrid. Here, the magnitudes of the equivalent series resistance (ESR) of the PANI–GNR, PANI–GNR–CNT composites and the GNR–CNT hybrid are about 1.55, 1.31 and 1.04 Ω, respectively, which can be obtained from the *x*-intercept of the Nyquist plots, indicating that the resistance of the PANI has been efficiently decreased by incorporating the prepared carbonic materials, especially for the GNR–CNT hybrid.

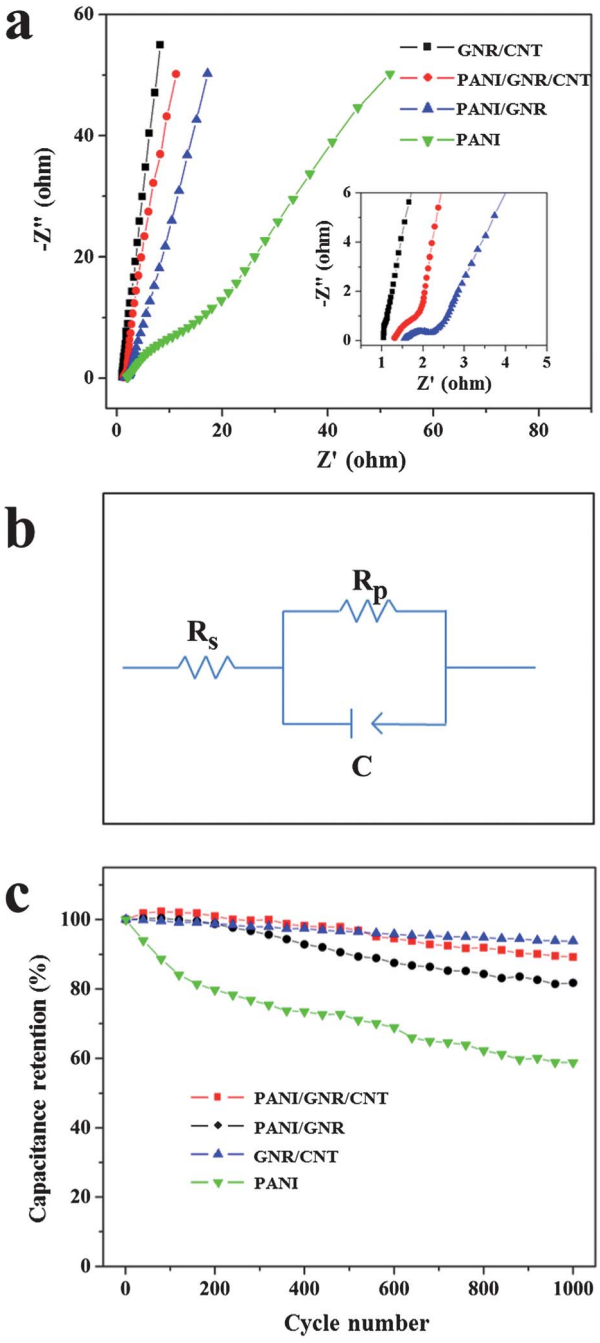

Fig. 7 (a) Impedance spectra of the neat PANI, GNR–CNT hybrid, PANI–GNR and PANI–GNR–CNT composite electrodes in 1 M H_2SO_4 solution measured at open circuit potential. (b) Electrical equivalent circuit used for fitting the impedance spectra. (c) Cycle life tests of the PANI, GNR–CNT hybrid, PANI–GNR and PANI–GNR–CNT composite electrodes measured at a current density of 1 A g^{-1}.

Here, the maximum power density of the device was calculated from the low frequency data of the impedance spectra from eqn (2):

$$P_{max} = V_i^2/(4m \times R) \quad (2)$$

Where V_i is the initial voltage, R is the ESR of the PANI–GNR–CNT composite, and m is the mass of the two electrodes. The maximum power density of the PANI–GNR–CNT composite-based supercapacitor is calculated to be about 29.6 kW kg^{-1}. Such a high value of power density demonstrates that the hierarchical PANI–GNR–CNT composite is well suited for powerful delivery applications, acting as a promising supercapacitor electrode material.[4,9]

The supercapacitor's performance can be strongly affected by all the components,[44] which have been represented in the form of an equivalent circuit, as seen in Fig. 7b. The circuit of the supercapacitor consists of an equivalent series resistance R_s representing the internal resistance of the supercapacitor, a capacitance C, and a parallel resistance R_p which is responsible for the self-discharge resistance of the supercapacitor. The long-term cycle stability is a crucial parameter for the electrode materials of supercapacitors. In this work, the long-term cycle life of the neat PANI, GNR–CNT hybrid and PANI–GNR–CNT composite was evaluated by repeating the charge–discharge tests for 1000 cycles at a current density of 1 A g^{-1}. The specific capacitance based on the electroactive materials as a function of cycle number is presented in Fig. 7c. It can be seen that the GNR–CNT hybrid electrode exhibits excellent stability over the entire cycle number range. Interestingly, the specific capacitance of the PANI–GNR–CNT composite initially increases at 1–200 cycles and then approximately holds steady, indicating that the composite is fully activated and reaches the optimum status during this process. Also, the PANI–GNR–CNT composite exhibits a superior stability by decreasing only 11% of its specific capacitance after 1000 cycles compared with 41% for the neat PANI, demonstrating that there is strong π–π interaction between the GNR–CNT hybrid and PANI, thus efficiently improving the long-term electrochemical stability. Here, the decrease of the specific capacitance can be attributed to the swelling and shrinkage of the PANI,[14,35] which may result in the deterioration of the conductivity and charge storage capability of conductive polymers during charge–discharge processes.[45]

Furthermore, the PANI–GNR–CNT composites with different mass ratios of PANI from 80 to 99 wt% have also been prepared and used as electrode materials. As seen in Fig. 8, the mass ratio of PANI has a significant influence on the specific capacitance of the PANI–GNR–CNT composites. The optimum content of PANI in the composites is about 95% with a maximum specific capacitance of 890 F g^{-1}. The composite with 99% PANI exhibits a lower specific capacitance of 461 F g^{-1}, which can be ascribed to the excessive and random stacking of PANI rod-like particles which are not fully and perfectly utilized during the charge–discharge processes. When the mass ratio of PANI is lower than 95%, on the other hand, the specific capacitance goes down, which can be attributed to more EDLC effects and less pseudocapacitor contributions in the PANI–GNR–CNT composite.

4 Conclusions

In summary, an electrode material of a PANI–GNR–CNT composite has been prepared by *in situ* polymerization of an aniline monomer on the surface of a GNR–CNT hybrid which is conveniently obtained by partially unzipping the CNTs. The introduction of GNRs or the GNR–CNT hybrid has greatly enhanced the properties of the PANI composite electrodes, such as charge transfer and ion transport. Interestingly, the presence of residual CNTs, which are not unzipped during the preparation of the GNRs, not only plays an important role in enhancing the electrical conductivity of the GNR–CNT hybrid but also results in a higher specific capacitance (890 F g^{-1}) of the PANI–GNR–CNT composite, compared with that (714 F g^{-1}) of the PANI–GNR composite, by acting as "bridges" between different GNRs or between the GNRs and PANI. The PANI–GNR–CNT composite maintains 89% of the initial specific capacitance after 1000 charge–discharge cycles, indicating an excellent electrochemical stability of the composite electrode. Due to the synergistic effect, these PANI–GNR–CNT composites with superior electrochemical properties may find potential applications in energy storage devices.

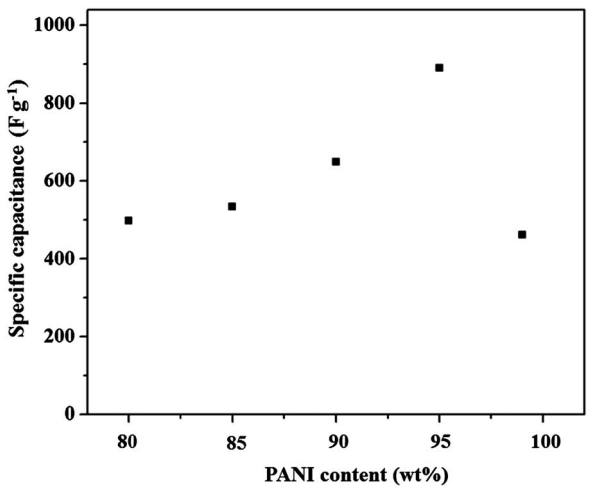

Fig. 8 Influence of the PANI content on specific capacitance of the PANI–GNR–CNT composite.

Acknowledgements

The authors are grateful for the financial support from the National Natural Science Foundation of China (51125011).

Notes and references

1 A. S. Arico, P. Bruce, B. Scrosati, J. M. Tarascon and W. Van Schalkwijk, *Nat. Mater.*, 2005, **4**, 366–377.
2 P. Simon and Y. Gogotsi, *Nat. Mater.*, 2008, **7**, 845–854.
3 L. L. Zhang and X. S. Zhao, *Chem. Soc. Rev.*, 2009, **38**, 2520–2531.
4 Y. Wang, Z. Q. Shi, Y. Huang, Y. F. Ma, C. Y. Wang, M. M. Chen and Y. S. Chen, *J. Phys. Chem. C*, 2009, **113**, 13103–13107.
5 H. X. Zhang, V. V. Bhat, N. C. Gallego and C. I. Contescu, *ACS Appl. Mater. Interfaces*, 2012, **4**, 3239–3246.
6 G. M. Wang, Y. C. Ling, F. Qian, X. Y. Yang, X. X. Liu and Y. Li, *J. Power Sources*, 2011, **196**, 5209–5214.
7 H. C. Gao, F. Xiao, C. B. Ching and H. W. Duan, *ACS Appl. Mater. Interfaces*, 2012, **4**, 7019–7025.
8 C. X. Guo, M. Wang, T. Chen, X. W. Lou and C. M. Li, *Adv. Energy Mater.*, 2011, **1**, 736–741.
9 C. X. Guo and C. M. Li, *Energy Environ. Sci.*, 2011, **4**, 4504–4507.
10 C. X. Guo, Y. Q. Shen, Z. L. Dong, X. D. Chen, X. W. Lou and C. M. Li, *Energy Environ. Sci.*, 2012, **5**, 6919–6922.
11 J. T. Zhang and X. S. Zhao, *J. Phys. Chem. C*, 2012, **116**, 5420–5426.
12 J. J. Xu, K. Wang, S. Z. Zu, B. H. Han and Z. X. Wei, *ACS Nano*, 2010, **4**, 5019–5026.
13 S. J. He, X. W. Hu, S. L. Chen, H. Hu, M. Hanif and H. Q. Hou, *J. Mater. Chem.*, 2012, **22**, 5114–5120.
14 J. Li, H. Q. Xie, Y. Li, J. Liu and Z. X. Li, *J. Power Sources*, 2011, **196**, 10775–10781.
15 B. Ma, X. Zhou, H. Bao, X. W. Li and G. C. Wang, *J. Power Sources*, 2012, **215**, 36–42.
16 J. W. An, J. H. Liu, Y. C. Zhou, H. F. Zhao, Y. X. Ma, M. L. Li, M. Yu and S. M. Li, *J. Phys. Chem. C*, 2012, **116**, 19699–19708.
17 H. L. Wang, Q. L. Hao, X. J. Yang, L. D. Lu and X. Wang, *Nanoscale*, 2010, **2**, 2164–2170.
18 D. Zhao, X. Y. Guo, Y. Gao and F. Gao, *ACS Appl. Mater. Interfaces*, 2012, **4**, 5583–5589.
19 Z. Q. Niu, P. S. Luan, Q. Shao, H. B. Dong, J. Z. Li, J. Chen, D. Zhao, L. Cai, W. Y. Zhou, X. D. Chen and S. S. Xie, *Energy Environ. Sci.*, 2012, **5**, 8726–8733.
20 S. Y. Yang, K. H. Chang, H. W. Tien, Y. F. Lee, S. M. Li, Y. S. Wang, J. Y. Wang, C. Ma and C. C. Hu, *J. Mater. Chem.*, 2011, **21**, 2374–2380.
21 Z. J. Fan, J. Yan, L. J. Zhi, Q. Zhang, T. Wei, J. Feng, M. L. Zhang, W. Z. Qian and F. Wei, *Adv. Mater.*, 2010, **22**, 3723.
22 Q. Su, Y. Y. Liang, X. L. Feng and K. Mullen, *Chem. Commun.*, 2010, **46**, 8279–8281.
23 A. L. Higginbotham, D. V. Kosynkin, A. Sinitskii, Z. Z. Sun and J. M. Tour, *ACS Nano*, 2010, **4**, 2059–2069.

24 D. V. Kosynkin, A. L. Higginbotham, A. Sinitskii, J. R. Lomeda, A. Dimiev, B. K. Price and J. M. Tour, *Nature*, 2009, **458**, 872–875.
25 J. Liu, A. G. Rinzler, H. J. Dai, J. H. Hafner, R. K. Bradley, P. J. Boul, A. Lu, T. Iverson, K. Shelimov, C. B. Huffman, F. Rodriguez-Macias, Y. S. Shon, T. R. Lee, D. T. Colbert and R. E. Smalley, *Science*, 1998, **280**, 1253–1256.
26 T. M. Wu, Y. W. Lin and C. S. Liao, *Carbon*, 2005, **43**, 734–740.
27 H. W. Wang, Y. L. Wang, Z. A. Hu and X. F. Wang, *ACS Appl. Mater. Interfaces*, 2012, **4**, 6826–6833.
28 V. C. Tung, L. M. Chen, M. J. Allen, J. K. Wassei, K. Nelson, R. B. Kaner and Y. Yang, *Nano Lett.*, 2009, **9**, 1949–1955.
29 J. Yan, T. Wei, B. Shao, Z. J. Fan, W. Z. Qian, M. L. Zhang and F. Wei, *Carbon*, 2010, **48**, 487–493.
30 M. Zhong, Y. Song, Y. F. Li, C. Ma, X. L. Zhai, J. L. Shi, Q. G. Guo and L. Liu, *J. Power Sources*, 2012, **217**, 6–12.
31 F. Yakuphanoglu, I. S. Yahia, G. Barim and B. F. Senkal, *Synth. Met.*, 2010, **160**, 1718–1726.
32 N. A. Kumar, H. J. Choi, Y. R. Shin, D. W. Chang, L. M. Dai and J. B. Baek, *ACS Nano*, 2012, **6**, 1715–1723.
33 J. H. Liu, J. W. An, Y. C. Zhou, Y. X. Ma, M. L. Li, M. Yu and S. M. Li, *ACS Appl. Mater. Interfaces*, 2012, **4**, 2870–2876.
34 X. B. Yan, J. T. Chen, J. Yang, Q. J. Xue and P. Miele, *ACS Appl. Mater. Interfaces*, 2010, **2**, 2521–2529.
35 T. M. Wu, Y. W. Lin and C. S. Liao, *Carbon*, 2005, **43**, 734–740.
36 X. J. Lu, H. Dou, S. D. Yang, L. Hao, L. J. Zhang, L. F. Shen, F. Zhang and X. G. Zhang, *Electrochim. Acta*, 2011, **56**, 9224–9232.
37 D. S. Yu and L. M. Dai, *J. Phys. Chem. Lett.*, 2010, **1**, 467–470.
38 Z. B. Yang, L. Li, Y. F. Luo, R. X. He, L. B. Qiu, H. J. Lin and H. S. Peng, *J. Mater. Chem. A*, 2013, **1**, 954–958.
39 T. Lee, T. Yun, B. Park, B. Sharma, H. K. Song and B. S. Kim, *J. Mater. Chem.*, 2012, **22**, 21092–21099.
40 Z. M. Cui, C. X. Guo, W. Y. Yuan and C. M. Li, *Phys. Chem. Chem. Phys.*, 2012, **14**, 12823–12828.
41 X. C. Dong, J. X. Wang, J. Wang, M. B. Chan-Park, X. G. Li, L. H. Wang, W. Huang and P. Chen, *Mater. Chem. Phys.*, 2012, **134**, 576–580.
42 Q. Wu, Y. X. Xu, Z. Y. Yao, A. R. Liu and G. Q. Shi, *ACS Nano*, 2010, **4**, 1963–1970.
43 M. D. Stoller, S. J. Park, Y. W. Zhu, J. H. An and R. S. Ruoff, *Nano Lett.*, 2008, **8**, 3498–3502.
44 E. Frackowiak and F. Beguin, *Carbon*, 2001, **39**, 937–950.
45 J. Yan, T. Wei, Z. J. Fan, W. Z. Qian, M. L. Zhang, X. D. Shen and F. Wei, *J. Power Sources*, 2010, **195**, 3041–3045.

